Clinical, Cosmetic and Investigational Dermatology

Dovepress

open access to scientific and medical research

Open Access Full Text Article

ORIGINAL RESEARCH

MicroRNA-182-5p Inhibits Hypertrophic Scar Formation by Inhibiting the Proliferation and Migration of Fibroblasts via SMAD4 Pathway

Mingzhu Jin[1], Xiao Xu[2]

[1]Department of Burns and Plastic Surgery, Fourth Medical Center of Chinese PLA General Hospital, Beijing, People's Republic of China; [2]Department of Ophthalmology, Third Medical Center of Chinese PLA General Hospital, Beijing, People's Republic of China

Correspondence: Xiao Xu, Email 13623345@qq.com

Introduction: Secondary to war wounds, trauma, etc., hypertrophic scar formation is the cause of an excessive proliferation of fibroblasts and accumulation of collagen fibers, which might affect cosmetic appearance, and could cause malignant transformation. miRNAs play an important role in disease regulation via inhibiting post-transcriptional protein translation by targeting and binding to the 3' UTR region of mRNA. Here we explore the mechanism and interventions of scar formation from the perspective of miRNA.

Methods: Hypertrophic scar-associated differential miRNAs were screened by analyzing sequencing data of normal skin and hypertrophic scar, and verified by RT-qPCR. Signaling pathways that may be influenced by differentially miRNAs were analyzed using KEGG and GO. miRNA mimics were used to explore the effects of miRNAs on SMAD signaling pathway proteins. Dual-luciferase assays were used to explore the targeted binding of miRNAs. The mimics of the miRNA were used to explore the impact of miRNAs on the proliferation, migration, apoptosis and collagen synthesis levels of hypertrophic scar fibroblasts. The scar model of rabbit ear was used to verify the influence of miRNA on wound healing and scar formation in vivo.

Results: Expression of miR-182-5p was found to be considerably decreased in hypertrophic scars and fibroblasts. miR-182-5p was found to act mainly by targeting the 3'UTR region of SMAD4, but not SMAD1 or SMAD3. miR-182-5p overexpression may drastically suppress the proliferation and migration of fibroblasts, accompanied by enhanced apoptosis and reduced collagen fiber synthesis. The overexpression of miR-182-5p in in vivo experiments could effectively inhibit hypertrophic scar formation without affecting the speed and quality of wound healing.

Conclusion: miR-182-5p inhibits hypertrophic scar formation by decreasing the proliferation and migration of fibroblasts via SMAD4 pathway, and is expected to become a novel hypertrophic scar therapeutic target.

Keywords: hypertrophic scar, microRNA, SMAD4, fibroblasts

Backgrounds

Secondary to war wounds, surgery, trauma, etc., wound healing depends on the continuous proliferation of fibroblasts and collagen synthesis in the dermis.[1,2] Skin scarring is considered as a natural outcome of the wound repair process. The incidence of scars after skin burns, trauma, and operations can be as high as 40% to 70%.[3] In the process of wound repair, many factors, such as collagen and proteoglycans, are involved in maintaining a dynamic balance in the synthesis and degradation of extracellular matrix (ECM). However, the abnormal synthesis of ECM typically results in the accumulation and remodeling of collagen tissue and leads to pathological skin scars. The pathogenesis of excessive ECM accumulation during wound healing includes genetics,[4] inflammation,[5] immune factors,[6] cytokines,[7] and other factors. When a scar does not resolve, uncontrolled chronic inflammation can persist and elicits excessive scarring that leads to a range of abnormal phenotypes such as hypertrophic and keloid scars. Unfortunately, the detailed mechanism responsible for hypertrophic and keloid scars is yet to be discovered.

Hypertrophic scar (HS), also characterized as connective tissue hyperplasia, is characterized by the excessive proliferation of fibroblasts and the ongoing hyperplasia of collagen anabolism during wound healing, leading to aberrant

Received: 21 November 2022
Accepted: 22 February 2023
Published: 8 March 2023

wound healing, and visible and elevated scars.[8–10] In contrast to normal skin (NS), hypertrophic scar (HS) is characterized by excessive proliferation of the dermal tissue, in a tumor-like growth mode, but HS generally did not extend the initial damage site unlike keloids.[11] The pathophysiology of hypertrophic scarring has been linked to several signaling pathways or cytokines, including epigenetic modification processes, S100A2, PI3K/Akt, TGF-β, and the SMAD pathway.[12–14] As the pathophysiology of HS remains unknown, new treatment targets must be identified via a rigorous understanding of the underlying processes of HS production.[15] The commonly used treatments for HS included surgical excision, radiation therapy, and intralesional corticosteroid injections such as triamcinolone acetonide and betamethasone, but they are accompanied by the possibility of recurrence. New treatments for HS need to be further explored and developed.[16]

MicroRNAs (miRNAs) are a family of endogenous, small, non-coding, single-stranded RNAs (about 22 nucleotides in length) that have been implicated in several biological processes, such as cell differentiation, proliferation, metastasis, and apoptosis.[17] miRNA is a novel regulator of fibroblast life processes, involved in cell proliferation and extracellular matrix (ECM) deposition associated with wound healing.[18–20] Meanwhile, miRNAs were founded to play an important role in HS, and miRNAs involved in fibroblast growth and collagen formation in HS have been identified and validated for their therapeutic effect on HS.[21,22]

We found that miRNA-182 plays a key role in a variety of fibrotic diseases, such as renal fibrosis, hepatic fibrosis, and myocardial fibrosis. Since hypertrophic scar is also a fibrotic disease, we hypothesized that miRNA-182 might be involved in the pathophysiological processes of hypertrophic scar. However, there were fewer systematic study on the role of miRNA-182 in hypertrophic scar. Therefore, we investigated whether miRNA-182 is involved in the regulation of hypertrophic scars. In this study, miRNA-182 with reduced expression in HS was screened by analyzing the results of miRNA sequencing array of HSs and NSs. We confirmed the reduced expression of miRNA-182-5p by RT-qPCR in HSs compared to NSs, also in hypertrophic scar-derived fibroblasts (HFs) compared to fibroblasts produced from normal skin (NFs). Further, the miRNA-182-5p-related signaling pathways and cellular functions were analyzed by KEGG and GO enrichment. Given the high correlation between miRNA-182-5p and SMAD signaling pathway, we investigated the impact of miRNA-182-5p on the SMAD protein family. miRNA-182-5p decreased SMAD4 expression by binding to the 3'UTR of SMAD4 mRNA, but had no impact on SMAD1 or SMAD3 expression. Moreover, in vitro experiments showed that miRNA-182-5p could inhibit the proliferation and migration of fibroblasts, with apoptosis enhanced. Through the scar model of rabbit ear, we confirmed in vivo that administration of miRNA-182-5p analogs during wound healing could inhibit hypertrophic scar formation.

Materials and Methods

Ethics Statement

The Ethics Committee of PLA General Hospital's Fourth Medical Center examined and approved the human sample study procedure. All patients were advised about the experimental techniques and research goals and volunteered to participate. For all patient samples, written informed permission was acquired. Animal studies were carried out in accordance with the Fourth Medical Center of PLA General Hospital's Guide for the Care and Use of Laboratory Animals, and were authorized by the Animal Care Committee of the Fourth Medical Center of PLA General Hospital.

Acquisition and Processing of Clinical Samples

Human skin samples were collected from patients undergoing surgery at the Department of Burns and Plastic Surgery, Fourth Medical Center of PLA General Hospital in Beijing, China. Totally, 12 HS tissues with their adjacent normal skin tissues (Table 1) were collected with an average age of 38.12±12.56 years old. None of the patients had previously received systemic or topical therapy. The collected samples were kept in sterile phosphate-buffered saline (PBS) and transported at 2–8 °C to the laboratory for processing. After rinsing with pre-chilled PBS, 50 mg of tissue was snap-frozen in liquid nitrogen and ground to a homogeneous state with a pre-chilled tissue grinder for RT-qPCR or Western Blot. The remained tissues were preserved for primary fibroblasts extraction and culture.

Table 1 The Profile of Each Involved Patients

Sample	Gender	Age (Years)	Biopsy Site	Etiology	Duration of HSs (Months)
NF/HF 1	Male	26	Upper extremity	Burn	4
NF/HF 2	Female	48	Abdomen	Surgery	6
NF/HF 3	Male	33	Thigh	Burn	10
NF/HF 4	Male	28	Neck	Burn	3
NF/HF 5	Male	27	Neck	Burn	4
NF/HF 6	Male	48	Neck	Trauma	9
NF/HF 7	Male	28	Armpit	Burn	4
NF/HF 8	Male	57	Neck	Burn	4
NF/HF 9	Female	44	Perineum	Surgery	80
NF/HF 10	Male	55	Scalp	High voltage electronic injury	3
NF/HF 11	Female	44	Upper arm	Burn	24
NF/HF 12	Female	20	Thigh	Burn	36

Isolation and Culture of Skin Fibroblasts

Patients' samples were washed three times with pre-chilled PBS before being chopped into tiny pieces (about 1 mm in diameter) and incubated in 0.1 mg/mL collagenase type I solution at 37 °C for 2hr to separate fibroblasts.[18,19] The fibroblasts were then pelleted and cultured in 10-cm culture plates with DMEM medium supplemented with 10% FBS, and incubated at 37 °C with 5% CO_2. Unless otherwise specified, fibroblasts produced during the third passage were utilized in all studies in this work.

Cell Transfection

The mimics and negative control (NC) of miRNA-182-5p were purchased from Guangzhou RiboBio Co., Ltd.[23] The third passage cells grew to 30–40% confluence in the six-well plates, then they were randomly divided into groups according to the random number table method, and the corresponding synthetic oligonucleotides were transfected into fibroblasts with Lipofectamine RNAiMAX (13778150, Thermo Fisher) respectively. After 48 hr of transfection, cells were collected for further experiments.

Histological Analysis

Tissue samples of NSs and HSs were trimmed to remove subcutaneous adipose tissue and then fixed in 4% paraformaldehyde, embedded in paraffin, sectioned into 5-μm thickness (UC7, Leica), mounted on slides, and performed HE staining (G1120, Solarbio) and MASSON staining (G1346, Solarbio) following the instructions. Images were acquired with an inverted phase contrast microscope (HY7800, Hitachi).

Western Blot

Proteins were isolated from tissues and cells according to the procedure for Western blot using RIPA lysate (89901, Thermo Fisher).[21] The lysate was centrifuged at 13,000 g for 10 min after being lysed on ice for 10 min. The supernatant was transferred to a fresh EP tube, and protein quantities were determined using a bicinchoninic acid (BCA) protein assay kit (PC0020, Solarbio). The lysate was boiled for 5 min in loading buffer containing sodium dodecyl sulfate (SDS) (P1040, Solarbio). After that, 45 μg samples were added into a 10% SDS-polyacrylamide gel electrophoresis (PAGE) gel (PG01010, Solarbio) before being transferred to polyvinylidene difluoride (PVDF) membranes (IPVH00010, Millipore). The membranes were treated with matching primary antibodies overnight at 4 °C after being blocked for 1 hr with 3% non-fat milk in TBST (pH 7.6). The membranes were then treated for 2 hr at room temperature (RT) with the appropriate horseradish peroxidase (HRP)-conjugated secondary antibodies. Following the antibody incubations, three 5-min TBST washes were performed. The protein bands were identified using ChemiDoc XRS chemiluminescence imaging equipment (BioRad), quantified using Image Lab (BioRad), and normalized to GAPDH levels. The procedure was repeated six times for tissues and three times for cell samples. All antibodies used were as follows: GAPDH Rabbit Ab (5174, 1:1000,

CST), Collagen I Rabbit Ab (81375, 1:1000, CST), Collagen III Rabbit Ab (63034, 1:1000, CST), SMAD1 Rabbit Ab (6944, 1:1000, CST), SMAD3 Rabbit Ab (9523, 1:1000, CST), SMAD4 Rabbit Ab (46535, 1:1000, CST), Bax Rabbit Ab (14796, 1:1000, CST), Bcl2 Rabbit Ab (3498, 1:1000, CST), HRP-conjugated Goat Anti-Rabbit IgG (H+L) (SA00001-2, 1:1000, Proteintech).

Real-Time Quantitative Polymerase Chain Reaction (RT–qPCR)

The collected skin samples or the pre-treated cells were rinsed with pre-chilled PBS before being collected in Trizol lysis buffer (DP419, TIANGEN). Total RNA and miRNA were extracted using the RNA extraction kit (DP419, TIANGEN) and the miRcute miRNA isolation kit (DP501, TIANGEN) according to the manufacturer's instructions. Nanodrop 2000 was used to determine total RNA or miRNA concentration, purity and quality. According to the manufacturer's instructions, cDNA was produced with the genome removed (KR118, TIANGEN). In addition, stem-loop reverse transcription procedures for miRNA were performed. Using the CFX96 real-time PCR equipment (BioRad, USA), quantitative PCR (qPCR) was done using RealUniversal Color PreMix (SYBR Green) (FP201, TIANGEN) and miRcute Plus miRNA qPCR Kit (SYBR Green) (FP411, TIANGEN). For the relative quantification of miRNA, U6 was used as the housekeeping gene. The qPCR reactions were carried out in triplicate. The Ct value was used to determine relative gene expression. Sangon Biotech (Shanghai) Co., Ltd. generated the primers. Table 2 shows the sequences of reverse transcription primers and fluorescence quantitative primers.

Bioinformatics Analysis

miRNA-182-5p-related signaling pathways were enriched via Kyoto Encyclopedia of Genes and Genomes (KEGG) and Gene Ontology (GO) analysis to find functional KEGG and GO annotations assisted and performed by Guangzhou RiboBio Co., Ltd.

Luciferase Reporter Assay

The SMAD4 3'UTR wild-type (WT) or mutant (MUT) with miRNA-182-5p binding sequences was amplified and cloned into the pHS-AVC-ZQ480 and pHS-AVC-ZQ481 luciferase reporter vector to synthesize SMAD4-WT or -MUT luciferase reporter vector by Beijing Syngentech Co., LTD. TransIntro EL transfection reagent was used to co-transfect the HFs with the respective WT or MUT vectors (FT201, TransGen). Following 48 hr of transfection, the Dual-Lucy Assay Kit (D0010, Solarbio) was used to measure luciferase activity using a microplate reader (Synergy2, BioTek) according to the manufacturer's recommendations.

Table 2 Sequences of Reverse Transcription Primers and Fluorescence Quantitative Primers

Symbol	Primer	Sequence (5'-3')
miR-182-5p	RT-Primer	GTCGTATCCAGTGCAGGGTCCGAGGTATT CGCACTGGATACGACAGTGTG
	F-Primer	GCGTTTGGCAATGGTAGAACT
	R-Primer	GTGCAGGGTCCGAGGT
miR-182-3p	RT-Primer	GTCGTATCCAGTGCAGGGTCCGAGGTATTC GCACTGGATACGACTAGTTG
	F-Primer	GTCAGTGGTTCTAGACTTGC
	R-Primer	GTGCAGGGTCCGAGGT
U6	RT-Primer	AACGCTTCACGAATTTGCGT
	F-Primer	CTCGCTTCGGCAGCACA
	R-Primer	AACGCTTCACGAATTTGCGT

Cell Proliferation

The impact of miRNA-182-5p on the proliferation of HFs was studied using the sulforhodamine B (SRB) test (ab235935, Abcam).[22] In summary, 10^4 cells were seeded onto sterile 96-well plates containing 100 μL of DMEM media with 10% FBS and incubated for 8 hr for cell adhesion, with 6 wells in each group. The wells were then rinsed with PBS, refilled with new medium, and co-transfected for 48 hr with matched synthetic oligonucleotides. The cells were then fixed with pre-cooled trichloroacetic acid and incubated for 1 hr at 4 °C. The plates were then cleaned three times with deionized water and dyed for 25 min at RT with SRB dye (0.4% dissolved in 1% acetic acid). Wells were rinsed three times with 1% acetic vinegar to remove any unbound color before drying in the air at RT. To solubilize the attached dye, 100 μL of Tris (10 mM) base was added to each well and gently stirred to achieve a homogeneous solution. Finally, absorbance was measured using a microplate reader (Synergy2, BioTek) at 510 nm according to the manufacturer's recommendations. The optical density (OD) values of each group were compared to the control group.

Cell Migration Assays

Transwell tests were used to assess the migratory characteristics of fibroblasts. In brief, 10^4 HFs were suspended in FBS-free media and seeded into the top chamber of a 24-well Transwell plate fitted with an 8.0 μm polycarbonate membrane. The bottom chamber was then filled with DMEM media (with FBS) treated with FGF. After 24 hr, the cells on the top side of the filter were wiped clean, and the cells that had migrated to the bottom surface were stained for 30 min with crystal violet (Solarbio, 0.1%, w/v). A light microscope was used to examine and count stained cells.

Cell Apoptosis

To detect cell apoptosis, fibroblasts were prepared and stained according to the manufacturer's instructions using the Annexin V-FITC Apoptosis Detection Kit I (556547, BD). Following 48 hr of co-transfection with matched synthetic oligonucleotides, the fibroblasts were harvested and resuspended in 1 Annexin V binding solution. Then annexin V-FITC and PI were introduced. The cells were identified by a FACScalibur equipment after 15 min of incubation (BD Biosciences). The experiment was carried out three times independently. The apoptosis rate of each group was computed as the total of the ratios of early and late apoptosis and compared with the control group using Flowjo software (TreeStar, USA).

Rabbit Ear Scar Model

Rabbit ear scar models were created in accordance with the literature.[23] SPF (Beijing) Biotechnology Co., Ltd. provided 12 mature New Zealand white male rabbits (2.0–2.5 kg). At the Fourth Medical Center of PLA General Hospital, all rabbits were kept in a special pathogen-free (SPF) microisolator environment with constant temperature (23 °C), humidity (60%), and a 12 hr light/dark cycle. Prior to wounding, rabbits were sedated with 1% pentobarbital (1.5 mg/kg) and the ear skin was swabbed with EtOH. Depilation was done, and full-thickness excisions were made with 10 mm biopsy punches until the cartilage on the ventral side of each ear was revealed. As a result, each rabbit had six wounds in each ear. The epidermis, dermis, and perichondrium were fully removed from each incision. After that, the wound was wrapped with sterile gauze for one day. The wounds were randomly assigned to one of three groups: Saline, miR-182-5p Agomir negative control (NC), or miR-182-5p Agomir. Each group had six wounds at each time point. For the direct application of drug to the wound bed would flow away from the wound surface after the animals wake up from anesthesia, which will inevitably affect the effect of the drug. So, the drug was applied via the injection at the edge of the wound. Every other day, Saline (50 μL), miR-182-5p Agomir NC (50 μL), or miR-182-5p Agomir (50 μL) were injected around the wounds using a micro syringe at four locations (12.5 μL each site). Furthermore, all rabbits were maintained in an SPF facility and fed SPF food and water throughout the trial. They were inspected once every day. In order to avoid the influence of local-regional effect during the experiment, all the wounds of each rabbit ear were treated with the same drug. In order to ensure the reliability of the experiment, all the animals were ensured to be consistent in age and body weight. To ensure the randomness of the experiment, we numbered and randomized the ears on each side. In addition, the injection of the drug was also performed blindly.

On postoperative days 0, 14, 28, and 28+14, the wounds were acquired and repaired surgically after the rabbits were euthanized by being overly injected with pentobarbital. At indicated time point, the ears of rabbits in each group were observed and recorded, and the wound healing rate was calculated. The wound healing rate was analyzed with ImageJ software.[24,25] In order to show the most natural wound healing process, we would take and display pictures with the scabbing retained. When calculating the wound healing rate, we would first remove the scabbing to fully expose the wound surface, then take pictures and use ImageJ for calculation. Wound healing rate (%) = (original wound area - unhealed wound area)/original wound area × 100%. The acquired samples were cut into 5-μm slices after embedded in paraffin tissue, and then stained with HE staining, MASSON staining, and Sirius Red staining.

Epithelization was assessed in HE staining through epithelial extension and coverage of the wound.[24,25] The thickness of the new epithelium was measured by ImageJ to reflect whether the quality of wound healing was affected by drug intervention.[26] The scar elevation index (SEI) was calculated to quantify the extent of hypertrophic scarring by two pathologists in six different randomly chosen high-power microscopic fields in HE-stained slides.[27] The SEI is defined as the ratio of the length of a perpendicular line on the scar tissue determined from the cartilage on the basis of the top point of the epithelium lining scar surface in micrometers to the perpendicular line determined between the intact ear cartilage and intact surface epithelium.[27] For MASSON staining, ImageJ was used to calculate the collagen volume fraction based on previously reported literature.[17,28] The percentage of collagen in the dermis was calculated by the ratio of the collagen-positive area to the total area of the dermis. Specifically, the Masson Trichrome function of the Color Deconvolution plugin in ImageJ was employed to separate collagen fibers from the background. After the Threshold was adjusted to ensure that the collagen was all correctly selected, the area of the collagen fibers was measured and compared to the total area of the dermis. Percentage of collagen (%) = collagen-positive area/total area of dermis × 100%. Sirius Red staining was further performed to determine changes in collagen content and type. The procedures were carried out in accordance with NIH guidelines and methods authorized by the IACUC.

Statistical Analysis

The data in the manuscript were all quantitative data and conformed to the normal distribution, thus presented as the mean ± SD. For data satisfying the homogeneity of variance, two independent samples *t*-test and One-way ANOVA with Tukey-post-hoc test were performed. For data not satisfying the homogeneity of variance, Mann–Whitney *U* or Kruskal–Wallis *H* rank-sum test were performed. The analysis was carried out blindly using the SPSS program (IBM, USA). The 0.05 level of confidence was regarded as a significant difference for all statistical tests.

Results

Increased Fibroblasts and Collagen Accumulation in Hypertrophic Scar

As a fibroproliferative disease, HSs usually caused by an irregular wound healing process after skin injury.[24] They are characterized by overproduction of extracellular matrix (ECM) such as collagens, and abnormal proliferation of fibroblasts.[29] Via HE staining and Masson staining (Figure 1A), we found that the number of fibroblasts and the degree of collagen deposition in normal skin were significantly lower than those in HSs. Further, Western Blot confirmed that the content of Collagen III and Collagen I in HSs was respectively 2.99 times and 2.27 times higher than those in NSs (Figure 1B, $P<0.01$).

Scar Formation-Related miRNA Screening

The mechanism exploration related to hypertrophic scar mainly involves the oxidative stress and inflammatory response of fibroblasts. In recent years, the role of miRNAs in the process of HS has become a research hotspot. Yamashita and his team performed miRNA microarray analysis to compare miRNA expression profiles between HFs and NFs (Table 3), and revealed the key role of miR-196a in collagen deposition in HFs by targeting the 3' untranslated region (UTR) of Collagen III and Collagen I.[21] Based on this, we further explored the second-ranked down-regulated miR-182 to explore its effect on fibroblast traits and HS formation.

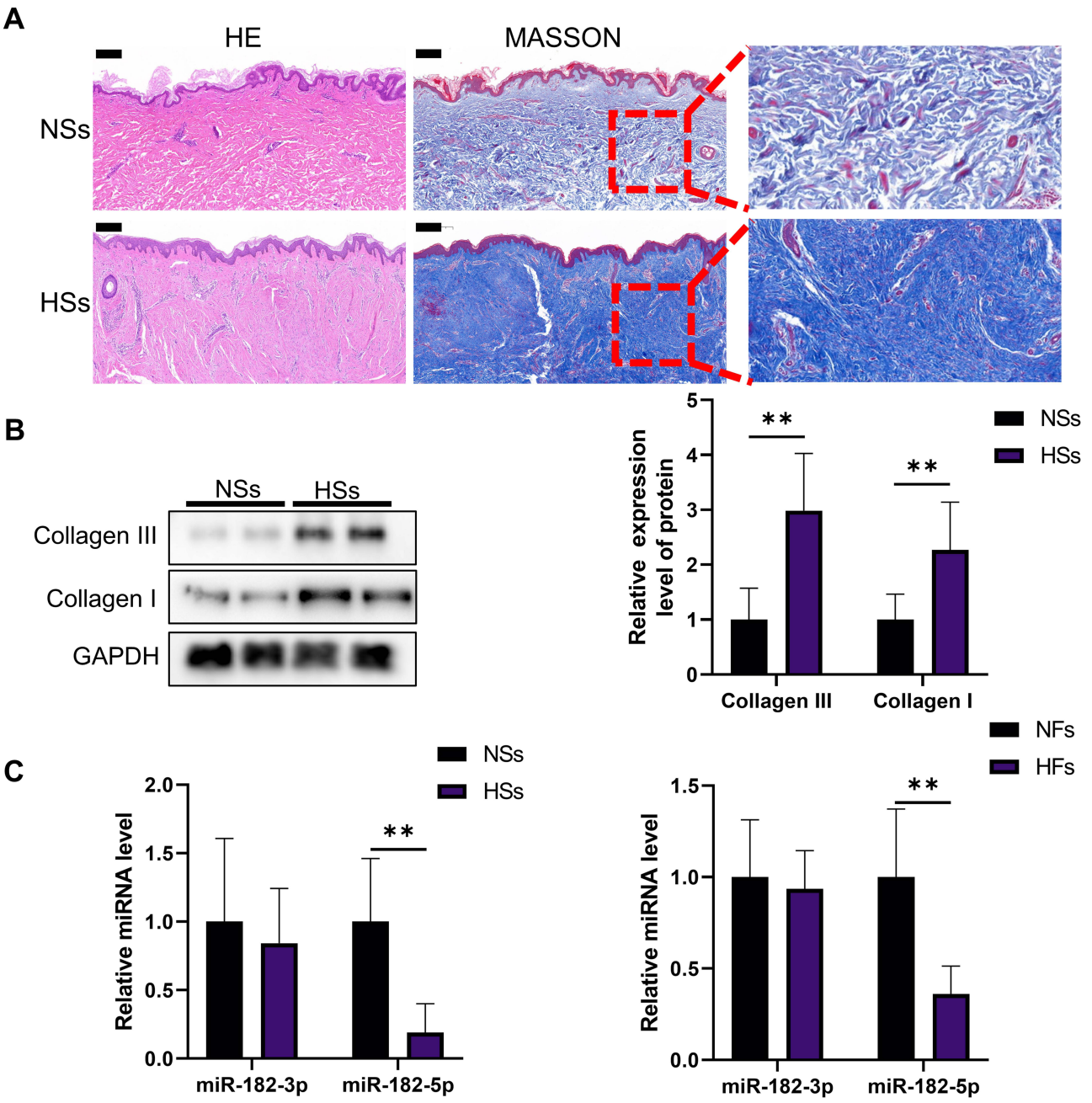

Figure 1 Expression levels of miR-182-5p in hypertrophic scar tissues and fibroblasts. (**A**) HE staining and Masson staining of NSs and HSs from clinical cases. The box area on the right side of each photomicrograph shows an enlarged version of the red square. Scale bar=200 μm. (**B**) Western blot was used to measure the expression level of Collagen III and Collagen I of NSs and HSs from clinical cases. N=6. ***P*<0.01. (**C**) RT-qPCR was employed to detect the expression levels of miR-182-3p and miR-182-5p in HSs tissues and fibroblasts, compared with the normal skin. N=6 for the skin tissues and N=3 for the fibroblasts. ***P*<0.01.

miR-182 has two types, respectively miR-182-3p and miR-182-5p. RT-qPCR revealed that the content of miR-182-3p in HS was similar to that in normal skin (Figure 1C), while the content of miR-182-5p was significantly reduced to 0.19 times in HS than in normal skin (Figure 1C, $P<0.01$). Further detection of fibroblasts derived from HS and NS found that there was no statistical difference in the expression level of miR-182-3p in HFs compared with NFs (Figure 1C), but an obvious decline in the expression level of miR-182-5p was observed in HFs (Figure 1C, $P<0.01$).

Table 3 Down-Regulated miRNAs in Scar Tissues

Down-Regulated miRNA	Fold Change (KF / NF)
hsa-miR-196a	0.093
hsa-miR-182	0.169
hsa-miR-452	0.188
hsa-miR-196b	0.246
hsa-miR-595	0.29
hsa-miR-769-5p	0.331
hsa-miR-30a	0.362
hsa-miR-224	0.373
hsa-miR-31	0.425
hsa-miR-31	0.433
hsa-miR-98	0.508
hsa-let-7f	0.54
hsa-miR-93	0.541
hsa-miR-30e	0.543
hsa-let-7a	0.545
hsa-miR-24	0.553
hsa-miR-331-3p	0.578
hsa-let-7d	0.6
hsa-miR-574-3p	0.628
hsa-miR-23a	0.634

Abbreviations: HF, hypertrophic scar derived fibroblast; miRNA, microRNA; NF, normal fibroblast.

Screening of the Binding Targets of miR-182-5p

Given that miRNAs may affect many proteins and related-signaling pathways, we further analyzed the most likely targets of miR-182-5p by KEGG (Figure 2A). We found that the SMAD pathway is mostly closely related to miR-182-5p with $P<0.01$. Further, we screened SMAD pathway-related proteins that miR-182-5p might affect via DIANA, miRTarBase, miRNAMap, TargetScan, and microRNA databases. It is predicted that miR-182-5p may bind to the 3'UTR regions of SMAD1, SMAD3 and SMAD4 (Figure 2B). After transfected with miR-182-5p mimics, we found that it could significantly increase the expression of miR-182-5p in HFs (Figure 2C). So Western Blot was arranged to further detect the effect of miR-182-5p overexpression on the expression of SMADs. As shown in Figure 2D, the miR-182-5p manifested inhibition on SMAD4 ($P<0.01$) but not SMAD1 or SMAD3. To confirm the hypothesis, luciferase reporters containing the miR-182-5p binding site on the SMAD4 3'UTR were constructed and we found that the miR-182-5p mimic reduced the luciferase activity of the SMAD4-WT reporter vector but not the SMAD4-MUT reporter vector in HFs.

Effects of miR-182-5p on Fibroblasts

SRB experiment showed that miR-182-5p mimics showed no obvious effect on the proliferation of HFs at 24 hr, but significantly inhibited the cell proliferation of HFs at 48 hr and 72 hr compared to the control group and NC group ($P<0.05$, Figure 3A). Meanwhile, the Transwell experiments showed that, the migratory capacity of HFs decreased after 48 hr incubation of miR-182-5p mimic ($P<0.01$, Figure 3B). In addition, the overexpression of miR-182-5p also increased the apoptosis of HFs, which may be meaningful in the remission of hypertrophic scar formation ($P<0.01$, Figure 3C). miR-182-5p mimics could regulate the apoptosis of HFs by promoting the expression of BAX ($P<0.01$) and meanwhile inhibiting the expression of Bcl2 ($P<0.01$, Figure 3D). Also, overexpression of miR-182-5p significantly inhibited the Collagen I and Collagen III synthesis in HFs ($P<0.01$), which further suggested that miR-182-5p may help to inhibit HS in the process of wound healing (Figure 3D).

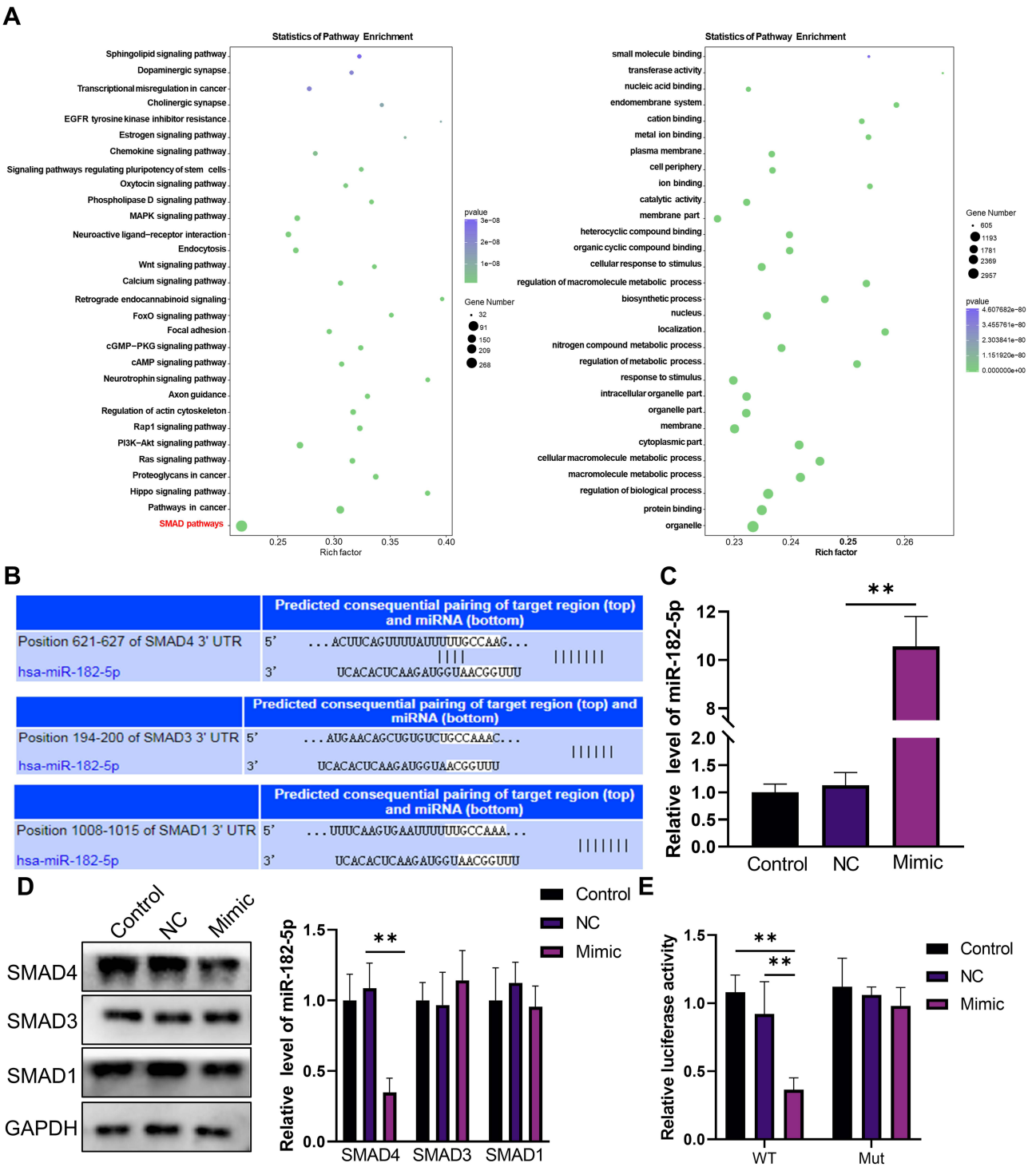

Figure 2 Screening of the binding target of miR-182-5p. (**A**) Analysis of signaling pathways that miR-182-5p may affect by KEGG (the left) and GO (the right) enrichment. (**B**) Analysis of the binding site of miR-182-5p to SMADs protein. (**C**) RT-qPCR was applied for the detection of expression level of miR-182-5p after HFs were incubated with miR-182-5p mimic. N=3. ***P*<0.01. (**D**) Western Blot was used to detect the effect of miR-182-5p on the protein expression level of SMADs in HFs. N=3. ***P*<0.01. (**E**) The dual-luciferase assay was used to detect the specific binding of miR-182-5p to the 3' UTR region of SMAD4. N=3. ***P*<0.01.

Effects of miR-182-5p Agomir on Wounds Healing and Hypertrophic Scar Formation

Further, we investigated the effect of miR-182-5p on wound healing and scar formation via in vivo experiments by rabbit ears HS models. As shown in Figure 4A, we established a full-thickness skin defect model with a diameter of 10 mm on the rabbit ear, with perichondrium exposed. Agomir is a double-stranded small RNA that has been specially labeled and

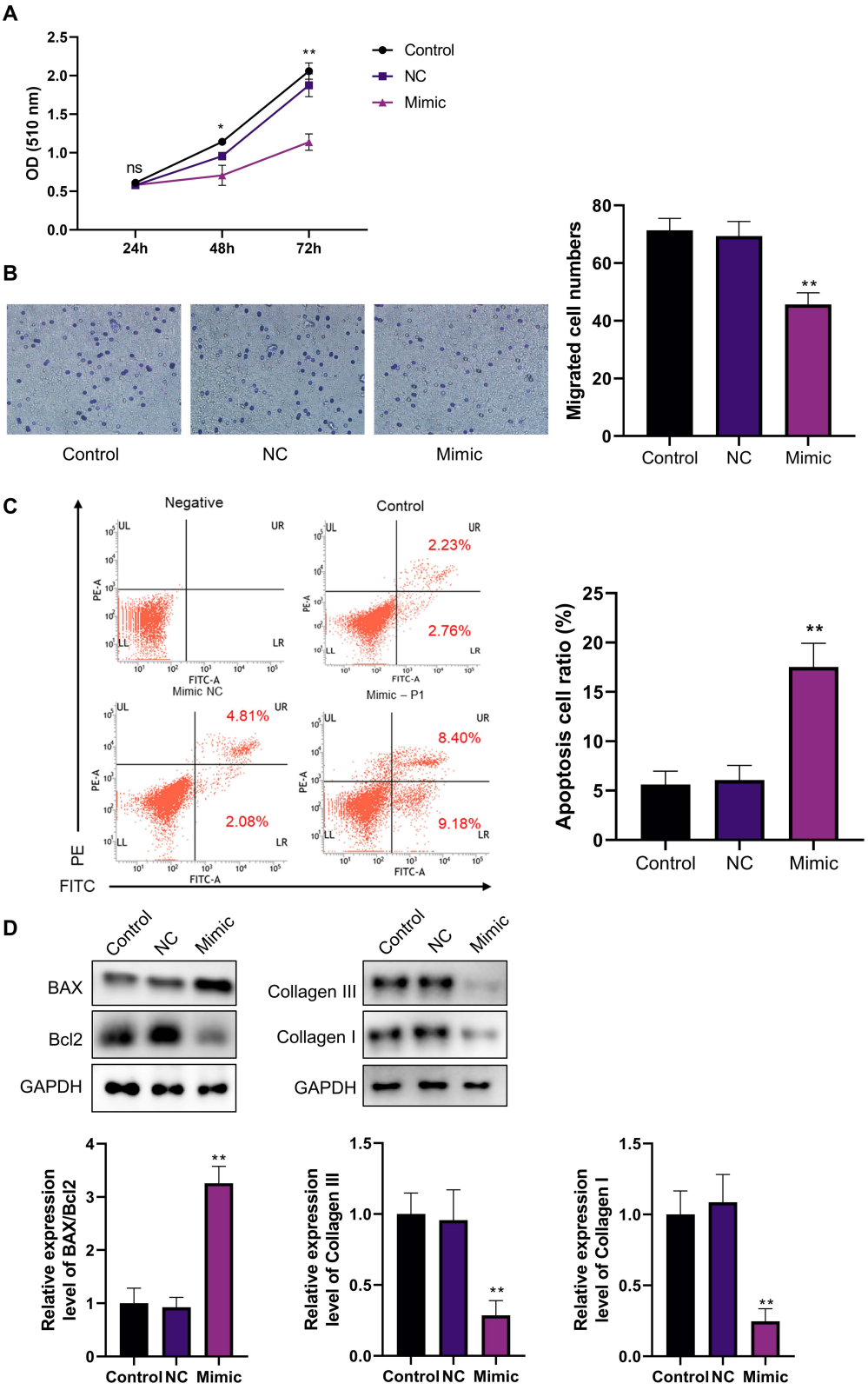

Figure 3 Effects of miR-182-5p on the characterization of HFs. (**A**) SRB assay was used to detect the effect of miR-182-5p on the proliferation ability of HFs. N=3. *P<0.05, **P<0.01. (**B**) Transwell assay was used to detect the effect of miR-182-5p on the migration ability of HFs. N=3. **P<0.01. (**C**) Annexin V-FITC assay was used to detect the effect of miR-182-5p on the apoptosis of HFs. N=3. **P<0.01. (**D**) Western Blot was performed for detection of the apoptosis-related proteins, Collagen III and Collagen I. N=3. **P<0.01.

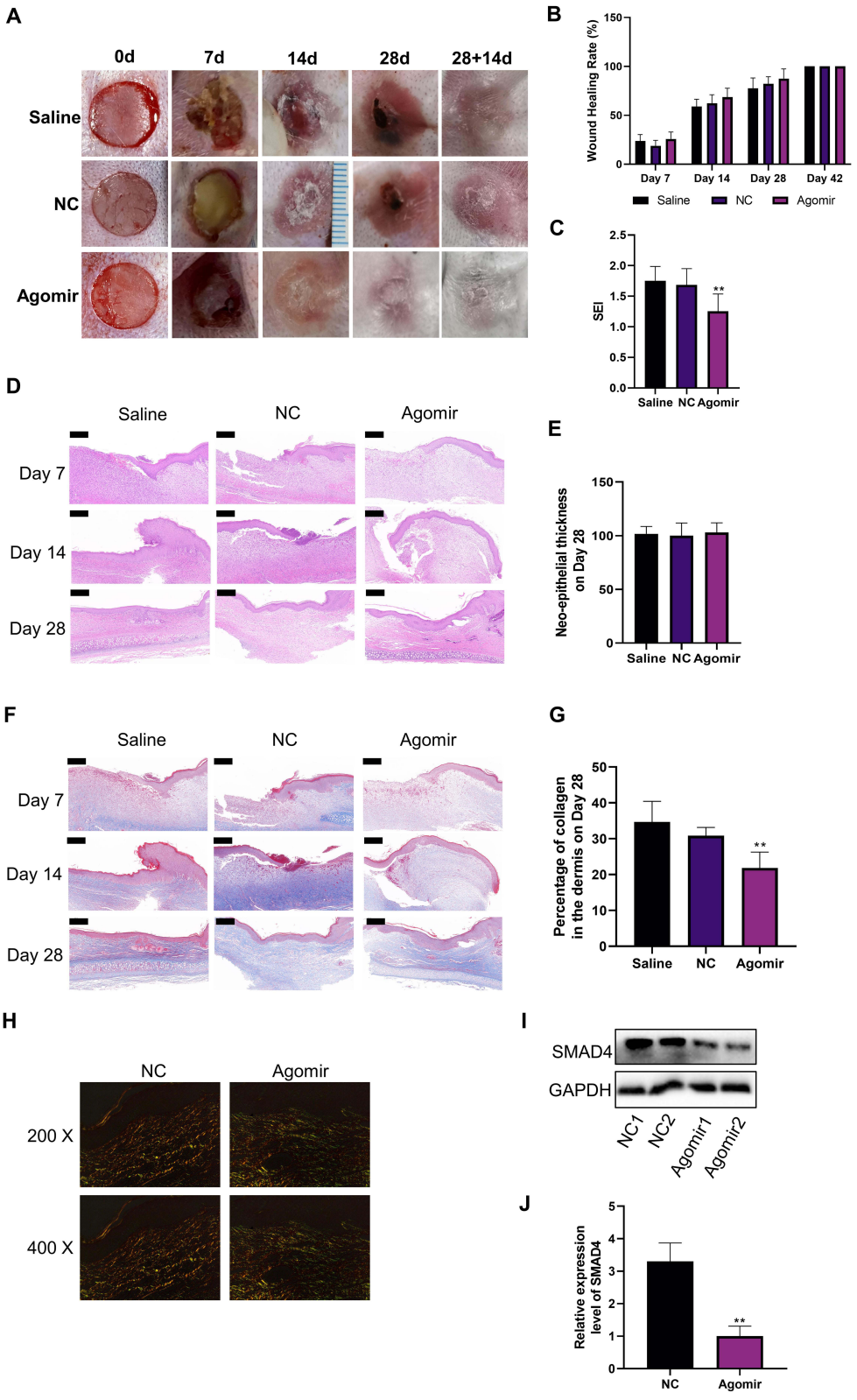

Figure 4 In vivo experiments on the effect of miR-182-5p on wound healing and hypertrophic scar formation. (**A** and **B**) Representative pictures of the process of wound healing and hypertrophic scar formation. The wound healing rate of groups were compared with the assistance of ImageJ. N=6. (**C**) The scar elevation index (SEI) was evaluated at postoperative day 28+14 to quantification of the hypertrophic scar formation. N=6. ***P*<0.01. (**D** and **E**) HE staining was used to evaluate the histology during wound healing. The neo-epithelial thickness was assessed on day 28 post-injury. N=6. Scale bar=200 μm. (**F** and **G**) Masson staining was used to evaluate the collagen deposition during wound healing. The percentage of collagen in the dermis was assessed on day 28 post-injury. N=6. ***P*<0.01. Scale bar=200 μm. (**H**) Sirius red staining was used to assess the collagen deposition on day 28+14 post-injury. N=6. Representative images from 200x and 400x polarized light microscopes were shown here. (**I** and **J**) Western Blot was performed to detect the changes in SMAD4 expression levels among groups on day 28+14 post-injury. N=6. ***P*<0.01.

chemically modified. It modulates the biological function of target genes by mimicking endogenous miRNAs, and is widely used for the intervention of target miRNAs in in vivo experiments.[30] As shown in Figure 4B, compared with the Saline group and the NC group, the miR-182-5p Agomir group had no statistical difference in the wound healing rate, which indicated that miR-182-5p Agomir had no obvious effect on the wound healing process. At postoperative day 28 +14, the miR-182-5p Agomir group showed improved scar formation compared to the other groups (Figure 4A). The hypertrophic scar formation was quantified, and SEI showed that the hypertrophic scar in the Agomir group had a lower bulge height than that in the Saline and NC groups (Figure 4C).

The results of HE staining revealed the wound healing process and scar formation process of each group from the point of pathology (Figure 4D). Specifically, during the wound healing process, along with the continuous formation of granulation tissue, the new epidermis continued to advance toward the center of the wound and gradually covered the granulation tissue. The cells of the new epidermis in each group were arranged neatly and clearly layered, the cytoplasm and nucleus were well colored, and the thickness of each layer of the epidermis had no obvious difference among groups. Inflammatory cell infiltration around blood vessels was seen in the dermis of each group, a large number of fibroblasts proliferated, and a number of new capillaries were seen in the dermis. The miR-182-5p Agomir group showed a similar wound healing process as the other groups (Figure 4D). On postoperative day 28, there was almost no inflammatory cell infiltration in the dermis of each group (Figure 4D). And there was no statistical difference in the neo-epithelial thickness (Figure 4E).

Masson staining was used to show collagen deposition during wound healing. As shown in Figure 4F, the content of collagen fibers in the dermis of the miR-182-5p Agomir group was lower than that of the Saline group and the NC group on the postoperative day 28. This effect persisted until postoperative day 28, when the percentage of collagen fibers in the dermis of the miR-182-5p Agomir group was still the lowest (Figure 4G). This may indicate that miR-182-5p could inhibit the formation of scar by inhibiting collagen deposition in the dermis during the wound healing process on the premise of the wound healing rate ensured. We further assessed dermal collagen fiber deposition by Sirius red staining (Figure 4H). With the injection of miR-182-5p Agomir, qualitative evaluation revealed that the content of Collagen I was decreased accompanied with the improvement of Collagen III (Figure 4H). Finally, we took the HSs of this time point and found that the expression of SMAD4 in the miR-182-5p Agomir group was significantly reduced, than that of the NC group (Figure 4I and J).

Discussion

As a disease closely associated with fibrous tissue growth, hypertrophic scar mainly caused by excessive proliferation of fibroblasts and deposition of collagen, which may be related to oxidative stress or hypoxia induction of fibroblasts. Hypertrophic scar and tumor are similar in several respects: uncontrolled cell proliferation, a hypoxic cellular micro-environment, and a disturbed balance between the epithelium and the mesenchyme. According to the research, miR-182-5p may build a mutual inhibitory circuit with FOXF2, which is linked to the metastasis of breast cancer.[31] miR-182-5p also exerts its anticancer effects in renal cancer cells via the Notch signaling pathway.[32] Wnt/β-catenin pathway plays an important role in the transformation of the mesenchymal and the epithelial cells, which is important to the wound healing and epithelial regeneration process.[33,34] Otherwise, miR-182-5p might enhance Wnt/β-catenin signaling by inhibiting the degradation of β-catenin and strengthening the roles of transcription factors of TCF4, which is mediated by the suppression of FOXO3a.[35] Given the similarities between HSs and tumor development, it is advantageous to investigate the relationship between miR-182-5p and HS formation.

In this study, we found that the expression of miR-182-5p was decreased in both HSs and HFs. Through the KEGG and GO analysis of the miR-182-5p related signaling pathways, it was found that miR-182-5p was closely related to the SMAD signaling pathway, which plays a key role in the HSs formation. miR-182-5p mimics showed a significant inhibitory effect on the expression of SMAD4 in HFs, but not the SMAD1 or SMAD3. By mutating the 3'UTR region, dual-luciferase experiments confirmed the targeted binding of miR-182-5p to the 3'UTR region of SMAD4. Moreover, we found that miR-182-5p could inhibit the proliferation and migratory abilities of HFs, accompanied by enhanced apoptosis. Western Blot showed that miR-182-5p could increase the BAX/Bcl2 ratio of HFs, and decrease the expression of Collagen I and Collagen III. From in vitro experiments, we preliminarily verified the possible mechanism by which

miR-182-5p may inhibit scar hyperplasia, namely inhibiting the proliferation of HFs, inducing their apoptosis, and inhibiting the synthesis of collagen fibers. By using Agomir of miR-182-5p in the process of wound healing, we found that compared with the control group and Agomir NC group, Agomir group did not show a decrease in wound healing rate, that is, Agomir did not affect or delay wound healing. This may be for the following reasons: SMAD4 mainly affects fibroblasts rather than epidermal stem cells. So the overexpression of miR-182-5p mainly affects fibroblasts rather than epidermal stem cells. Meanwhile, the expression level of miR-182-5p in normal fibroblasts are higher than that in scar fibroblasts, namely, there is enough miR-182-5p in normal fibroblasts to suppress SMAD4 expression, so SMAD4 expression in normal skin will not be affected by the overexpression of miR-182-5p by Agomir. Therefore, miR-182-5p can promote scar-free healing process mainly by responding expression of miR-182-5p in scar fibroblasts, without affecting the wound healing process significantly, which is the basis and premise for its further anti scar treatment. Furthermore, we observed the synthesis of extracellular matrix, especially collagen, in the process of scar formation by Masson staining, to determine the effect of Agomir on rabbit ear scar model. We found that Agomir can effectively inhibit the deposition of collagen fibers in the process of scar formation, which is manifested by more sparse collagen fiber arrangement and less collagen fiber deposition in the Agomir group. After 28+14 days of drug intervention, the scar volume of the Agomir group was significantly smaller and softer than that of the negative control group and saline group. At the same time, we further stained type I and III collagen fibers by Sirius red staining, which further confirmed the inhibition of Agomir on collagen fiber deposition during scar formation. In addition, the detection of the protein content of SMAD4 also proves that Agomir inhibits the expression of SMAD4, that is, Agomir plays its anti-scar role by the inhibition of SMAD4 expression.

Research on miRNAs has been increasing in recent years, ranging from tissue regeneration to targeted therapy of tumors.[36–38] miRNAs can interfere with the normal translation of mRNAs by targeting the 3'UTR region of mRNAs, thereby playing a role in post-transcriptional modification.[39,40] This study preliminarily explored the preventive and therapeutic effects of miR-182-5p on scarring prevention. However, the molecular mechanism of miR-182-5p in scars and the ceRNA regulation mechanism of miR-182-5p need to be further explored.[41] Also, future studies can explore the improvement of miRNA-related delivery methods, such as loading miRNA-related drugs into microneedles or hydrogels for delivery, which may further improve the efficacy.[42–44]

Limitations

Although the rabbit ear model of HS is relatively simple, with good repeatability and a high degree of standardization, it also has many limitations. First of all, due to the difference in immune system between the rabbits and humans, the rabbit ear model cannot be used to identify the immunopathogenic factors in the formation of HS. Meanwhile, the genetic susceptibility that plays an important role in human scars can also not be studied through this model.[45] Secondly, for the rabbit ear skin is very thin and clings to the surface of the cartilage without muscle and subcutaneous tissue, scarring occurs on the surface of cartilage without blood vessels, which is also different from human scarring.[46] Third, differences in lipid metabolism have been shown to play a role in scar formation. However, rabbits are herbivorous animals, and their lipid metabolism characteristics may be different from those of humans, which may affect its scar formation.[47]

Conclusions

Our findings show that miR-182-5p has an inhibitory impact on fibrosis in HFs and scar formation through the SMAD4 pathway. The proliferation, apoptosis and migration may be related to the inhibitory effect of miR-182-5p on scar formation. In vivo experiments confirmed that our method can inhibit scar formation without affecting the speed and quality of wound healing, which is a promising therapeutic direction.

Data Sharing Statement

Further information and requests for reagents may be directed to and will be fulfilled by the Lead Contact: X.X.

Ethics Approval and Consent

This study was performed in compliance with the principles of the Helsinki Declaration and Guidelines for the Care and Use of Laboratory Animals of the Chinese Institute of Health. All procedures using animals were approved by the Animal Research Committee and Ethics Committee of General Hospital of PLA. The use of human skin samples was approved by the Ethics Committee of General Hospital of PLA. We obtained the written informed consent from all the patients participated in this study.

Acknowledgments

Thanks to the involved volunteers who provided tissues for the study. We would like to thank Prof. Minliang Chen for his contribution to this manuscript. We would like to thank Dr. Jiachen Sun for his contribution to the revision of the manuscript.

Author Contributions

X.X. conceptualized the study, designed experiments, critically reviewed the manuscript, reviewed and agreed on all versions of the article before submission and during revision, agreed to take responsibility and be accountable for the contents of the article. M.J. performed experiments, collected, and analyzed the data. All authors contributed to data analysis, drafting or revising the article, have agreed on the journal to which the article will be submitted, gave final approval of the version to be published, and agree to be accountable for all aspects of the work.

Funding

There is no funding to report.

Disclosure

The authors declare that the research was conducted in the absence of any commercial or financial relationships that could be construed as a potential conflict of interest.

References

1. Fawcett S, Al Kassas R, M Dykes I, et al. A time to heal: microRNA and circadian dynamics in cutaneous wound repair. *Clin Sci*. 2022;136(8):579–597. doi:10.1042/CS20220011
2. Plikus MV, Guerrero-Juarez CF, Ito M, et al. Regeneration of fat cells from myofibroblasts during wound healing. *Science*. 2017;355(6326):748–752. doi:10.1126/science.aai8792
3. Kim S, Choi TH, Liu W, et al. Update on scar management: guidelines for treating Asian patients. *Plast Reconstr Surg*. 2013;132(6):1580–1589. doi:10.1097/PRS.0b013e3182a8070c
4. Marneros AG, Norris JEC, Watanabe S, Reichenberger E, Olsen BR. Genome scans provide evidence for keloid susceptibility loci on chromosomes 2q23 and 7p11. *J Invest Dermatol*. 2004;122(5):1126–1132. doi:10.1111/j.0022-202X.2004.22327.x
5. Akaishi S, Ogawa R, Hyakusoku H. Keloid and hypertrophic scar: neurogenic inflammation hypotheses. *Med Hypotheses*. 2008;71(1):32–38. doi:10.1016/j.mehy.2008.01.032
6. Chen Z, Zhou L, Won T, et al. Characterization of CD45RO+ memory T lymphocytes in keloid disease. *Br J Dermatol*. 2018;178(4):940–950. doi:10.1111/bjd.16173
7. Shih B, Garside E, McGrouther DA, Bayat A. Molecular dissection of abnormal wound healing processes resulting in keloid disease. *Wound Repair Regen*. 2010;18(2):139–153. doi:10.1111/j.1524-475X.2009.00553.x
8. Huang J, Zhou X, Wang W, et al. Combined analyses of RNA-sequence and Hi-C along with GWAS loci-A novel approach to dissect keloid disorder genetic mechanism. *PLoS Genet*. 2022;18:e1010168. doi:10.1371/journal.pgen.1010168
9. Chen L, Su Y, Yin B, et al. LARP6 regulates keloid fibroblast proliferation, invasion, and ability to synthesize collagen. *J Invest Dermatol*. 2022;142:2395–2405.e2397. doi:10.1016/j.jid.2022.01.028
10. Liang Y, Zhou R, Fu X, Wang C, Wang D. HOXA5 counteracts the function of pathological scar-derived fibroblasts by partially activating p53 signaling. *Cell Death Dis*. 2021;12(1):40. doi:10.1038/s41419-020-03323-x
11. Limandjaja GC, Belien JM, Scheper RJ, Niessen FB, Gibbs S. Hypertrophic and keloid scars fail to progress from the CD 34 − /α-smooth muscle actin (α- SMA) + immature scar phenotype and show gradient differences in α- SMA and p16 expression. *Br J Dermatol*. 2020;182(4):974–986. doi:10.1111/bjd.18219
12. Lv W, Ren Y, Hou K, et al. Epigenetic modification mechanisms involved in keloid: current status and prospect. *Clin Epigenetics*. 2020;12(1):183. doi:10.1186/s13148-020-00981-8
13. Lv W, Liu S, Zhang Q, et al. Circular RNA CircCOL5A1 sponges the MiR-7-5p/Epac1 axis to promote the progression of keloids through regulating PI3K/Akt signaling pathway. *Front Cell Dev Biol*. 2021;9:626027. doi:10.3389/fcell.2021.626027
14. Zhao J, Zhong A, Friedrich EE, et al. S100A12 induced in the epidermis by reduced hydration activates dermal fibroblasts and causes dermal fibrosis. *J Invest Dermatol*. 2017;137(3):650–659. doi:10.1016/j.jid.2016.10.040

15. Rang Z, Wang Z-Y, Pang Q-Y, et al. MiR-181a targets PHLPP2 to augment AKT signaling and regulate proliferation and apoptosis in human keloid fibroblasts. *Cell Physiol Biochem*. 2016;40(3–4):796–806. doi:10.1159/000453139
16. Yu X, Li Z, Chan MTV, Wu W. K. microRNA deregulation in keloids: an opportunity for clinical intervention? *Cell Prolif*. 2015;48(6):626–630. doi:10.1111/cpr.12225
17. Wei Q, Wang Y, Ma K, et al. Extracellular vesicles from human umbilical cord mesenchymal stem cells facilitate diabetic wound healing through MiR-17-5p-mediated enhancement of angiogenesis. *Stem Cell Rev Rep*. 2022;18(3):1025–1040. doi:10.1007/s12015-021-10176-0
18. Ma C, Qi X, Wei Y-F, et al. Amelioration of ligamentum flavum hypertrophy using umbilical cord mesenchymal stromal cell-derived extracellular vesicles. *Bioactive Mater*. 2023;19:139–154. doi:10.1016/j.bioactmat.2022.03.042
19. Xia W, Li M, Jiang X, et al. Young fibroblast-derived exosomal microRNA-125b transfers beneficial effects on aged cutaneous wound healing. *J Nanobiotechnology*. 2022;20(1):144. doi:10.1186/s12951-022-01348-2
20. Bian D, Wu Y, Song G, Azizi R, Zamani A. The application of mesenchymal stromal cells (MSCs) and their derivative exosome in skin wound healing: a comprehensive review. *Stem Cell Res Ther*. 2022;13(1):24. doi:10.1186/s13287-021-02697-9
21. Kashiyama K, Mitsutake N, Matsuse M, et al. miR-196a downregulation increases the expression of type I and III collagens in keloid fibroblasts. *J Invest Dermatol*. 2012;132(6):1597–1604. doi:10.1038/jid.2012.22
22. Gallant-Behm CL, Piper J, Lynch JM, et al. A MicroRNA-29 mimic (remlarsen) represses extracellular matrix expression and fibroplasia in the skin. *J Invest Dermatol*. 2019;139(5):1073–1081. doi:10.1016/j.jid.2018.11.007
23. Xu J-H, Zhao J-X, Jiang M-Y, et al. MiR-193 promotes cell proliferation and invasion by ING5/PI3K/AKT pathway of triple-negative breast cancer. *Eur Rev Med Pharmacol Sci*. 2020;24(6):3122–3129. doi:10.26355/eurrev_202003_20679
24. Sun J, Liu X, Shen C, Zhang W, Niu Y. Adiponectin receptor agonist AdipoRon blocks skin inflamm-ageing by regulating mitochondrial dynamics. *Cell Prolif*. 2021;54(12):e13155. doi:10.1111/cpr.13155
25. Sun J, Zhao H, Shen C, et al. Tideglusib promotes wound healing in aged skin by activating PI3K/Akt pathway. *Stem Cell Res Ther*. 2022;13(1):269. doi:10.1186/s13287-022-02949-2
26. de Souza TR, Souza AK, Garcia SB, et al. Photobiomodulation increases viability in full-thickness grafts in rats submitted to nicotine. *Lasers Surg Med*. 2020;52(5):449–455. doi:10.1002/lsm.23155
27. Demir CY, Ersoz ME, Erten R, et al. Comparison of enalapril, candesartan and intralesional triamcinolone in reducing hypertrophic scar development: an experimental study. *Aesthetic Plast Surg*. 2018;42(2):352–361. doi:10.1007/s00266-018-1073-6
28. Toss MS, Miligy IM, Gorringe KL, et al. Geometric characteristics of collagen have independent prognostic significance in breast ductal carcinoma in situ: an image analysis study. *Mod Pathol*. 2019;32(10):1473–1485. doi:10.1038/s41379-019-0296-7
29. Zhang Q, Shi L, He H, et al. Down-regulating scar formation by microneedles directly via a mechanical communication pathway. *ACS Nano*. 2022;16(7):10163–10178. doi:10.1021/acsnano.1c11016
30. Sun Y, Wang Q, Zhang Y, et al. Multigenerational maternal obesity increases the incidence of HCC in offspring via miR-27a-3p. *J Hepatol*. 2020;73(3):603–615. doi:10.1016/j.jhep.2020.03.050
31. Lu J-T, Tan -C-C, Wu X-R, et al. FOXF2 deficiency accelerates the visceral metastasis of basal-like breast cancer by unrestrictedly increasing TGF-β and miR-182-5p. *Cell Death Differ*. 2020;27(10):2973–2987. doi:10.1038/s41418-020-0555-7
32. Wang W, Hu W, Wang Y, et al. Long non-coding RNA UCA1 promotes malignant phenotypes of renal cancer cells by modulating the miR-182-5p/DLL4 axis as a ceRNA. *Mol Cancer*. 2020;19(1):18. doi:10.1186/s12943-020-1132-x
33. Sinnberg T, Levesque MP, Krochmann J, et al. Wnt-signaling enhances neural crest migration of melanoma cells and induces an invasive phenotype. *Mol Cancer*. 2018;17(1):59. doi:10.1186/s12943-018-0773-5
34. Liu X, Xie P, Hao N, et al. HIF-1–regulated expression of calreticulin promotes breast tumorigenesis and progression through Wnt/β-catenin pathway activation. *Proc Natl Acad Sci USA*. 2021;118(44):1. doi:10.1073/pnas.2109144118
35. Cao M-Q, You A-B, Zhu X-D, et al. miR-182-5p promotes hepatocellular carcinoma progression by repressing FOXO3a. *J Hematol Oncol*. 2018;11(1):12. doi:10.1186/s13045-018-0555-y
36. Hogdall D, O'Rourke CJ, Larsen FO, et al. Whole blood microRNAs capture systemic reprogramming and have diagnostic potential in patients with biliary tract cancer. *J Hepatol*. 2022;2022:3. doi:10.1016/j.jhep.2022.05.036
37. Cao M, Isaac R, Yan W, et al. Cancer-cell-secreted extracellular vesicles suppress insulin secretion through miR-122 to impair systemic glucose homeostasis and contribute to tumour growth. *Nat Cell Biol*. 2022;24(6):954–967. doi:10.1038/s41556-022-00919-7
38. Li J, Yao Y, Wang Y, et al. Modulation of the crosstalk between Schwann cells and macrophages for nerve regeneration: a therapeutic strategy based on a multifunctional tetrahedral framework nucleic acids system. *Adv Mater*. 2022;34(46):e2202513. doi:10.1002/adma.202202513
39. Komoll R-M, Hu Q, Olarewaju O, et al. MicroRNA-342-3p is a potent tumour suppressor in hepatocellular carcinoma. *J Hepatol*. 2021;74(1):122–134. doi:10.1016/j.jhep.2020.07.039
40. de Abreu RC, Fernandes H, da Costa Martins PA, et al. Native and bioengineered extracellular vesicles for cardiovascular therapeutics. *Nat Rev Cardiol*. 2020;17(11):685–697. doi:10.1038/s41569-020-0389-5
41. Zhu M, Liu J, Xiao J, et al. Lnc-mg is a long non-coding RNA that promotes myogenesis. *Nat Commun*. 2017;8(1):14718. doi:10.1038/ncomms14718
42. Sharma P, Kumar A, Agarwal T, et al. Nucleic acid-based therapeutics for dermal wound healing. *Int J Biol Macromol*. 2022;220:920–933. doi:10.1016/j.ijbiomac.2022.08.099
43. Elkhoury K, Chen M, Koçak P, et al. Hybrid extracellular vesicles-liposome incorporated advanced bioink to deliver microRNA. *Biofabrication*. 2022;14(4):045008. doi:10.1088/1758-5090/ac8621
44. Yu C, Chen L, Zhou W, et al. Injectable bacteria-sensitive hydrogel promotes repair of infected fractures via sustained release of miRNA antagonist. *ACS Appl Mater Interfaces*. 2022;14(30):34427–34442. doi:10.1021/acsami.2c08491
45. van den Broek LJ, Limandjaja GC, Niessen FB, Gibbs S. Human hypertrophic and keloid scar models: principles, limitations and future challenges from a tissue engineering perspective. *Exp Dermatol*. 2014;23(6):382–386. doi:10.1111/exd.12419
46. Ehrlich HP, Needle AL. Wound healing in tight-skin mice: delayed closure of excised wounds. *Plast Reconstr Surg*. 1983;72(2):190–198. doi:10.1097/00006534-198308000-00012
47. Yang J-X, Li S-Y, Chen M-L, He L-R. The role of altered fatty acid in pathological scars and their dermal fibroblasts. *Chin J Traumatol*. 2022;25(4):218–223. doi:10.1016/j.cjtee.2022.03.006